Frequency Measurement of Dynamic Stress in Polarization Maintaining Fibers
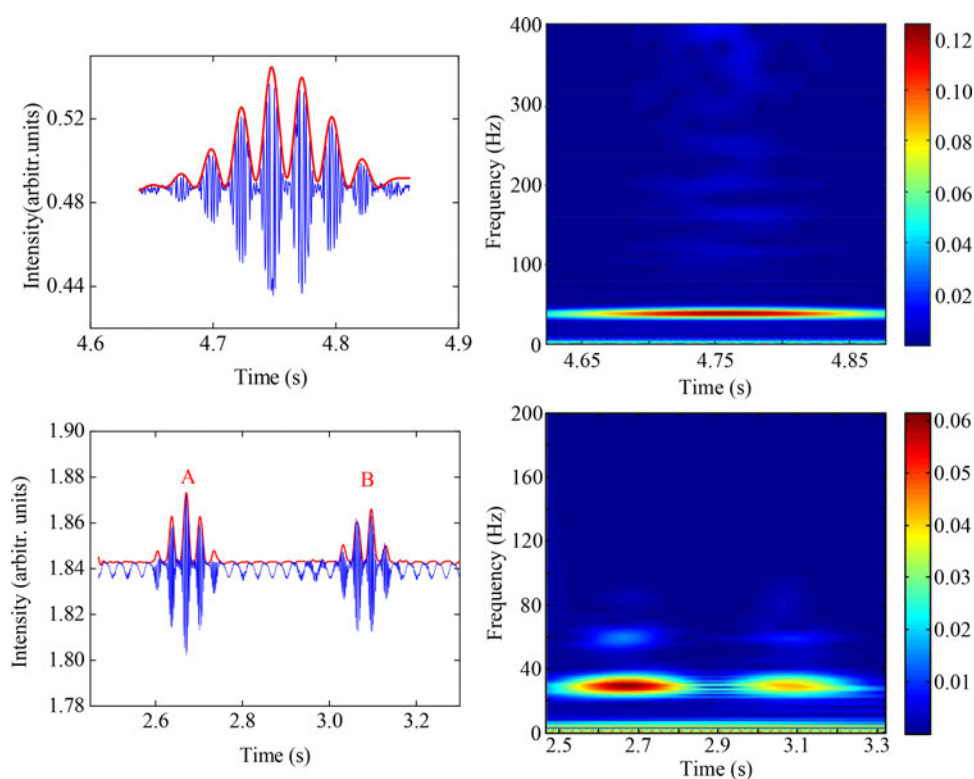
Hongxia Zhang
Yuyao Wang
Guoqiang Wen
Dagong Jia
Tiegen Liu

Frequency Measurement of Dynamic Stress in Polarization Maintaining Fibers

Hongxia Zhang [1,2] **Yuyao Wang** [1,2] **Guoqiang Wen** [1,3]
Dagong Jia [1,2] **and Tiegen Liu** [1,2]

[1]College of Precision Instrument and Optoelectronics Engineering, Tianjin University, Tianjin 300072, China
[2]Key Laboratory of Optoelectronics Information and Technical Science, EMC, Tianjin 300072, China
[3]Automobile & Rail Transportation School, Tianjin Sino-German University of Applied Sciences, Tianjin 300350, China

Abstract: Up to now, the distributed polarization coupling (DPC) measurement system based on white light interferometry (WLI) has been mainly studied for static and quasi-static measurement. In this paper, we developed the DPC system to measure the instantaneous frequency of dynamic stress. First, we set up a model of transversal stress on the panda polarization maintaining fiber (PMF) and simulated the interferograms of dynamic coupling points when the PMF is subjected to stress of cosine wave, sawtooth wave and square wave. Then, we did groups of experiments to measure the interferograms of dynamic coupling points, including cosinoidal coupling point, sawtooth wave coupling point, square wave coupling point, and two cosinoidal coupling points. By applying wavelet transform to the envelops of interferograms, we can obtain the time-frequency distribution images and demodulate the instantaneous frequency of external stress. The absolute error of experiments is less than 1.84 Hz. Finally, we deduced the upper and lower limits for frequency measurement and discussed the methods of enlarging the frequency range in detail. The method introduced in this paper has potential application in fiber sensing of dynamic stress.

Index Terms: Distributed polarization coupling (DPC), white light interferometry, polarization maintaining fiber (PMF), dynamic stress, wavelet transform, instantaneous frequency, time-frequency distribution.

1. Introduction

The distributed polarization coupling (DPC) measurement system based on white light interferometry (WLI) have been widely employed in the measurement of physical parameters such as stress [1], displacement [2] due to its wide dynamic range, high sensitivity and simple construction. In DPC measurement system, external perturbation such as micro-bending, twists, strains, stress will induce polarization coupling in polarization maintaining fiber (PMF). In previous researches, there are several methods to generate coupling points: principal axis misalignment at the adapter [3]; fusion splice point [4]; using specially designed clips to exert point-like lateral force [5]; or PMF wounded on a fiber spool with a thin metal rod to generate periodic transversal stresses at locations the fiber crossing the rod [6]. These methods can only induce static or quasi-static coupling points.
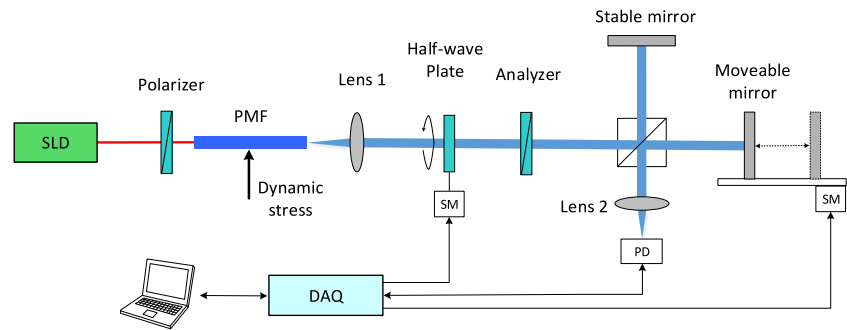
Fig. 1. Experimental setup of dynamic polarization coupling measurement system. SLD, superluminescent diode; PD, photodiode; SM, step motor; DAQ, data acquisition card.

However, in practical application such as intruder detection, evaluating structures of bridges, or oil pipeline leakage monitoring, the external disturbance are usually time-varying signals. Therefore, it is necessary to study dynamic polarization coupling in PMF.

Many other methods were proposed to measure dynamic stress. Fiber Bragg grating (FBG) sensors with different demodulation techniques received considerable research interests for dynamic stress sensing. For example, using a polarization maintaining fiber loop mirror [7] or a fiber Mach-Zehnder interferometer [8] which achieved 1 kHz and 2.5 kHz frequency measurement, respectively. However, this technology can be only used in single point or multipoint dynamic strain sensing rather than distributed sensing. Kazuo Hotate *et al*. proposed a correlation-based continuous-wave technique for dynamic strain measurements using stimulated Brillouin scattering [9]. Vibration at rates of up to 2 kHz can be measured by simply observing the Brillouin intensity variation at a fixed pump-probe frequency difference. But this technique is not suitable for long distance fiber sensing. Recently, A fiber vibration sensing technique based on a time-gated digital optical frequency domain reflectometry (TGD-OFDR) has been studied, with a measurable vibration frequency up to 600 Hz [10]. Nevertheless, the main drawback of such optical backscattering based sensors is that a high-power light source or additional components are usually required for enhancement of sensitivity since the scattered light is weak, and high-performance signal processing equipment is also needed for real-time measurements, which makes systems very expensive for application.

In this paper, a DPC measurement system for dynamic stress sensing is demonstrated. We first set up a model of transversal stress on PMF and simulated the interference signals when PMF is subjected to cosine wave stress, sawtooth wave stress and square wave stress, respectively. Then groups of experiments were conducted to verify the simulations. Hilbert transform and wavelet transform were used to extract envelop of coupling point and obtain time-frequency distribution image of envelop, respectively. In the end, we deduced the upper and lower limits for frequency measurement in our system, and came up with several methods to enlarge frequency range.

2. Principle

2.1 Experimental Configuration

The white light interferometry for dynamic polarization coupling measurement is shown in Fig. 1. The broadband light emitted by superluminescent diode (SLD) passes through the polarizer and then couples into the PMF with one polarization mode excited. The polarizer aligns to the fast axis of PMF. When light passes the coupling point caused by the dynamic stress, a fraction of light will couple to the orthogonal direction. As the excited mode and the coupling mode propagating along the PMF with different velocities, an optical path difference (OPD) appears between the two eigenmodes. After the lens 1, the angle between the polarization modes and the principal axis of the analyzer is rotated to 45 degree by the half-wave plate. And the analyzer is used to project two polarization modes onto the same direction. The scanning mirror of Michelson interferometer
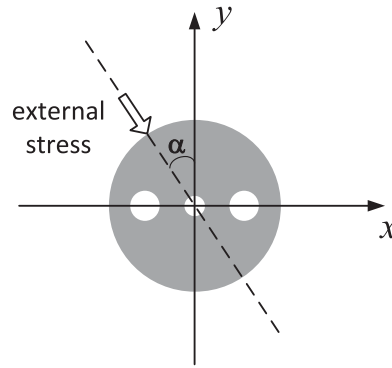
Fig. 2. Model of transversal stress on the panda PMF.

driven by step motor moves to compensate the OPD generated in PMF. Finally, the interference signal is detected by the photodiode.

2.2 Model of Transversal Stress on PMF

PMF is stress-induced birefringent fiber that is sensitive to external stress. Therefore, when an external stress is applied to PMF, the beat length of PMF will change at the stressed section. In the meantime, the magnitude of birefringence changes and the birefringence axes rotates by an angle with respect to those unstressed sections [11]. We take panda PMF for example and set up the model of transversal stress on the fiber, as shown in Fig. 2. We establish x, y coordinates according to the slow and fast axes when PMF does not subject to stress, the light propagates perpendicular to x-y plane. α is the angle between y-axis and the direction of external stress. Due to the rotation of birefringence axes, the power of two polarization modes couples with each other. The coupling strength h is given by:

$$h = F^2 \sin^2(2\alpha) \cdot \left\{ \frac{\sin\left[\pi\sqrt{1 + F^2 + 2F\cos(2\alpha)}\,(l/L_{b0})\right]}{\sqrt{1 + F^2 + 2F\cos(2\alpha)}} \right\}^2 \tag{1}$$

Here, l and L_{b0} represent the length and the beat length of stressed section, respectively. F is the normalized stress:

$$F = \frac{2n_y{}^3 L_{b0} f (1 + \mu)(p_{12} - p_{11})}{\pi \lambda r E} \tag{2}$$

Where f is the stress on the PMF per unit length, μ is the Poisson's ratio, p_{11} and p_{12} are strain optical coefficients, λ is the wavelength of light source, r is the radius of PMF, E is the elastic modulus, and n_y is refractive index of fast axis in the unstressed condition.

The two orthogonal modes propagate in the PMF with different velocities and interfere with each other at the output of scanning Michelson interferometer. The interference intensity I can be expressed as:

$$I = \frac{A^2}{4} \{1 + \gamma(\Delta Z) \cos(k\Delta z)$$

$$+ \sqrt{h(1-h)}\gamma(\Delta Z - \Delta n_b L) \cos(k(\Delta Z - \Delta n_b L))\} \tag{3}$$

Where $\gamma(\ )$ is the optical coherence function of the light source which is described by:

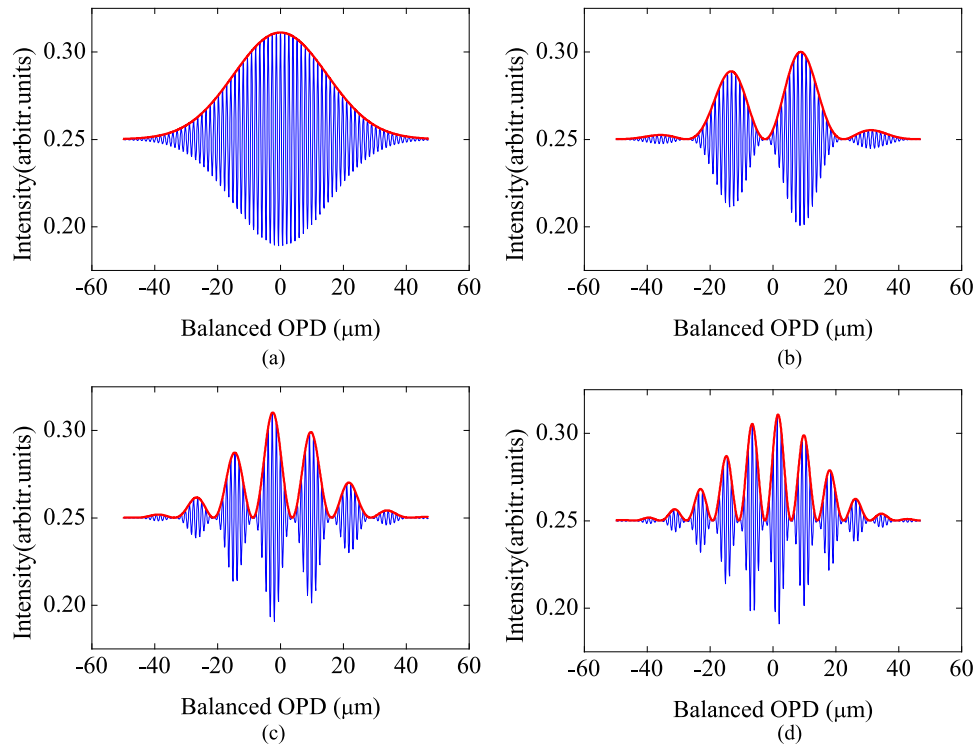$$\gamma(\Delta x) = \exp\left(-(2\Delta x/L_c)^2\right) \tag{4}$$

Fig. 3. Simulated interference fringes and envelops of cosinoidal dynamic coupling point with (a) $\upsilon = 0\,\text{Hz}$; (b) $\upsilon = 20\,\text{Hz}$; (c) $\upsilon = 40\,\text{Hz}$; (d) $\upsilon = 60\,\text{Hz}$.

In (3) and (4), A is the amplitude of electric field, k is the wave number, $\triangle Z$ is the OPD of Michelson interferometer, $\triangle n_b = n_x - n_y$, representing the refractive index difference of slow axis and fast axis, L is the distance between the coupling point and the output end of PMF, and L_c is the coherent length of light source.

It can be seen from (3) and (4) that there should be three interference fringes in the interference signal: a central interference fringe and two interference fringes induced by the dynamic coupling point. Since two interference fringes induced by dynamic coupling point are symmetrical about the central fringe, we only take the interference fringe on one side of the central fringe for frequency demodulation.

2.3 Simulation of Dynamic Coupling Points

According to (3), we simulate the interferograms of dynamic coupling point subject to external stress with different waveforms and different frequencies. In our simulation, the sampling rate of DAQ is 7500 Hz, the moveable arm of Michelson interferometer moves at 0.25 mm/s, the central wavelength and the coherent length of SLD are 1310 nm and 42 μm respectively, exactly corresponding to our experimental setup. The length of stressed section and the angle α are set as 3 mm and 45°, respectively. Firstly, we set the dynamic force f as cosine functions with different frequencies: $f = 1 + \cos(2\pi\upsilon t)$, where υ represents the frequency of external stress. The simulation results are shown in Fig. 3.

Fig. 3(a)–(d) are interferograms corresponding to the cosinoidal stress of 0 Hz, 20 Hz, 40 Hz and 60 Hz respectively. The red lines represent the interference envelops extracted by Hilbert transform[1]. Fig. 3(a) is a typical static interferogram whose envelop follows a Gaussian distribution, while in Fig. 3(b)–(d), the envelops of dynamic coupling points are modulated by coupling strength. As the frequency of external stress increases, the modulation frequency of envelop increases as well.
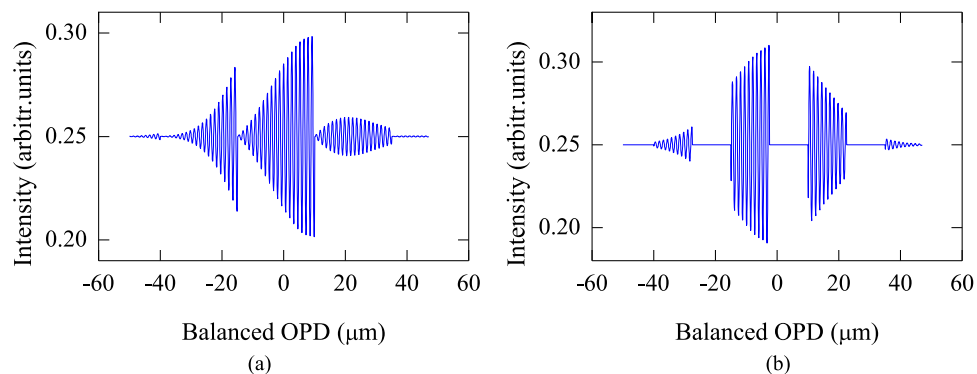
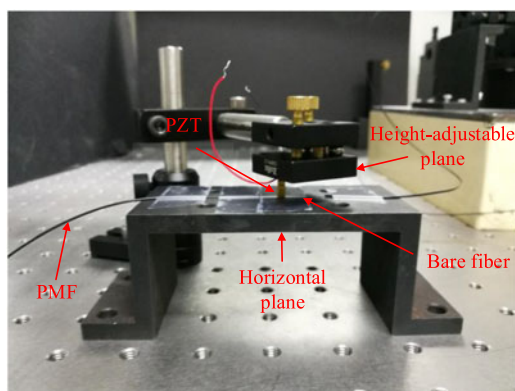Fig. 4. Simulated interference fringes of dynamic coupling points. (a) Sawtooth wave; (b) square wave.

Fig. 5. Device to exert a transversal force on PMF.

Then we simulated the interferograms of dynamic coupling point subject to stresses of sawtooth wave and square wave. The peak to peak values of external stresses are both set as 2 N/mm, and the frequencies are 20 Hz. The simulation results are shown in Fig. 4. It can be seen that the envelops are also modulated periodically by coupling strength.

In order to demodulate the frequency of external stresses from the interferogram measured in experiment, we need to apply time-frequency analysis to the envelops of interference signals. Wavelet transform is a good tool for time-frequency analysis which can reflect the instantaneous frequency of signal changing with time. We applied wavelet transform to the signal envelop to obtain the time-frequency distribution image which can describe how the spectral content of the signal changes with time [12]. The wavelet basis function we chose is Morlet wavelet.

3. Experimental Results

In order to measure the dynamic coupling point in PMF, we deployed the experimental setup depicted in Fig. 1 and conducted groups of experiments. The device to exert a transversal force on fiber is shown in Fig. 5. A PZT (Thorlabs, PK2JA2P2, 8.0 μm displacement, 3.0 mm × 3.0 mm × 9.0 mm outer dimension) driven by a function generator is used to exert a dynamic stress on PMF, sticking to a height-adjustable plane. The PMF with a beat length of 2.4 mm is stripped off the loose tube and the cladding at the stressed segment and fixed on a horizontal platform. We did groups of experiments including cosine wave stress, sawtooth wave stress, square wave stress and two dynamic coupling points. The experimental results are shown below.
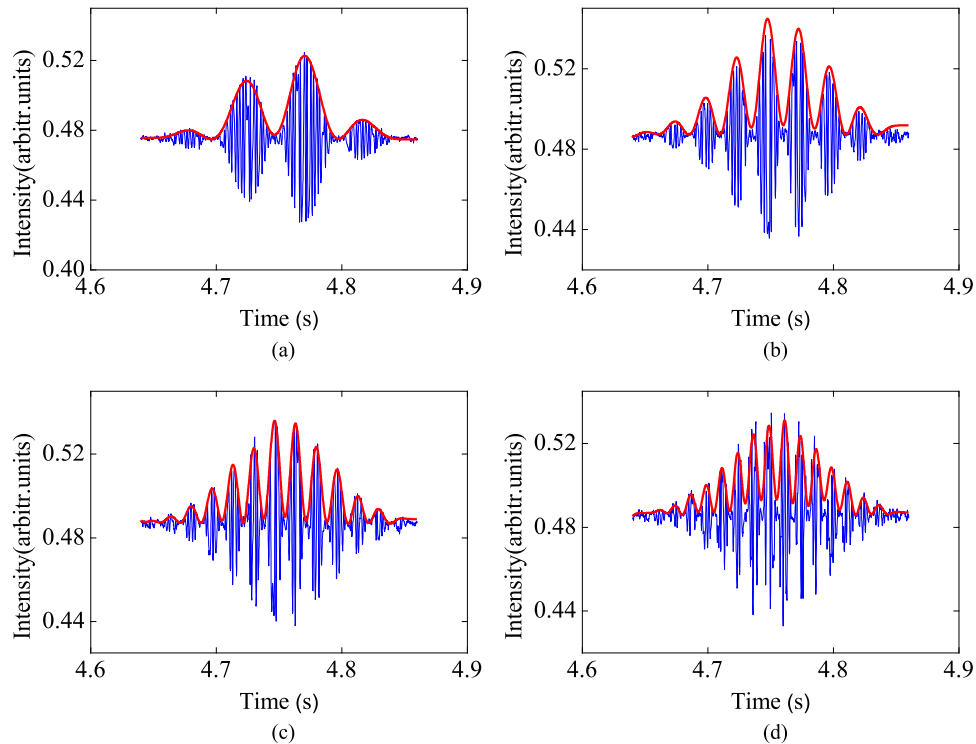
Fig. 6. Interferograms of cosinoidal coupling points in experiment. (a) $\upsilon = 20\,\text{Hz}$; (b) $\upsilon = 40\,\text{Hz}$; (c) $\upsilon = 60\,\text{Hz}$; (d) $\upsilon = 80\,\text{Hz}$.
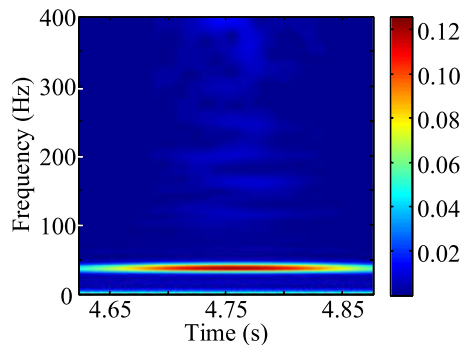

Fig. 7. The time-frequency distribution image of envelop in Fig. 5(b).

3.1 Measurement for Cosinoidal Stress

Fig. 6 shows the interferograms of coupling points subject to cosinoidal stresses. The frequencies of external stresses are 20 Hz, 40 Hz, 60Hz and 80 Hz in Fig. 6(a)–(d), and the amplitudes of function generator are 750 mV. The red lines are envelops extracted by Hilbert transform and denoised by Butterworth low-pass filters [13]. We can see that the envelops of interferograms are modulated periodically and the modulation frequency increases as the frequency of stress increases.

Fig. 7 shows the time-frequency distribution image of envelop in Fig. 6(b) by using wavelet transform. There are one frequency component whose central frequency is 40.38 Hz existing in Fig. 7 all the time, corresponding to the frequency of external stress. Different colors in Fig. 7 represent different signal amplitudes, it can be seen that the amplitude of envelop decreases from the centre to the edge.

By applying wavelet transform to the envelops of dynamic coupling points in Figs. 3 and 6, we can get the theoretical and experimental frequencies of envelops. We make the frequencies of external
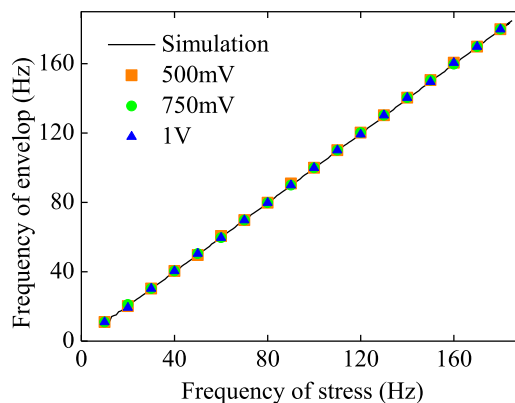
Fig. 8. The relationship between the frequency of external stress and the modulation frequency of envelop. The curve is the simulation result and the square, spot, triangle represent the measurement results with peak to peak value of driving voltage of 500 mV, 750 mV, 1 V respectively.

stresses change from 10 Hz to 180 Hz in simulation and obtain the relationship between the frequencies of envelops and the frequencies of external stresses, as shown in Fig. 8. The square, spot, triangle in Fig. 8 are the experimental results with frequencies from 10 Hz to 180 Hz and driving voltages of 500 mV, 750 mV, 1 V, respectively. We can see that the modulation frequency of envelop changes linearly with frequency of external stress and it is irrelevant to the peak to peak value of driving voltage. Three groups of experimental results are in good agreement with the simulation and the root-mean-square errors (RMSE) of experimental results for 500 mV, 750 mV and 1 V are 0.61 Hz, 0.48 Hz, 0.58 Hz respectively. The measurement error is relatively large when the frequency of force is less than 20 Hz, because there is a inherent frequency component of 2.753 Hz in each time-frequency distribution image, which will overlap with the measured frequency components and lead to measurement error. The maximum absolute errors are all 1.38 Hz and appear at the frequency of 10 Hz in three groups of experiments.

3.2 Measurement for Stress of Sawtooth Wave and Square Wave

In order to demonstrate that our method is not limited to measure cosine signal, we applied sawtooth wave stress and square wave stress to PMF and measured the interferograms. The frequencies of sawtooth wave and square wave are both 30 Hz and the voltage amplitudes of function generator are 250 mV and 400 mV respectively.

Fig. 9 shows the experimental results for sawtooth wave and square wave. Fig. 9(a) and (c) are interferograms for sawtooth wave and square wave, Fig. 9(b) and (d) are their corresponding time-frequency distribution images of envelops. Table 1 shows the comparison of theoretical and experimental results. The sawtooth wave consists of a fundamental frequency and harmonics whose frequency are integral multiple of fundamental frequency. And the square wave is made up of a fundamental frequency and higher harmonics which are odd times of fundamental frequency. In Fig. 9(b) and (d), some higher harmonics are too weak and submerged in the noises, so we could not observe it.The measurement errors for sawtooth wave stress and square wave stress are less than 1.84 Hz.

3.3 Measurement for Two Dynamic Coupling Points Simultaneously

The DPC system not only achieved single dynamic stress measurement, but also allows distributed dynamic stress sensing. When there are two dynamic stresses applied to the different positions of PMF, the OPDs generated by two dynamic stresses are different. With the moveable mirror of Michelson interferometer scanning, the OPDs can be compensated at different positions, which results in five interference fringes at different positions in the interferogram: one central interference
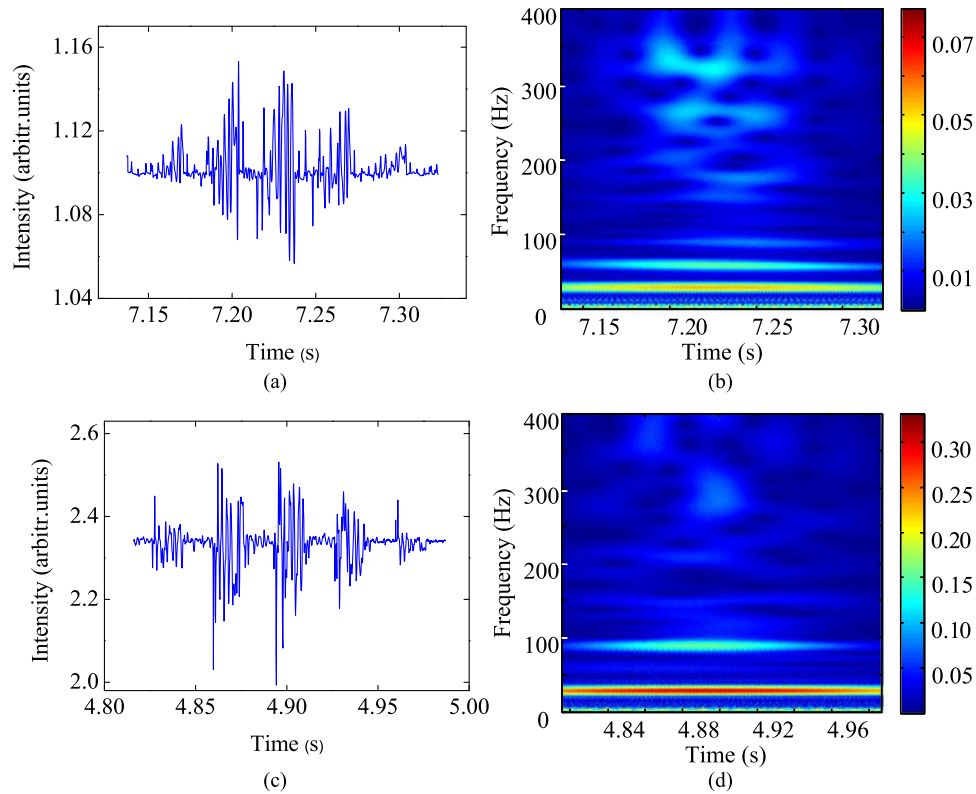
Fig. 9. Experimental results of sawtooth wave stress and square wave stress. (a) Interferogram of coupling point subject to sawtooth wave stress with frequency of 30 Hz; (b) Time-frequency distribution of envelop of signal in Fig. 9(a); (c) Interferogram of coupling point subject to square wave stress with frequency of 30 Hz; (d) Time-frequency distribution of envelop of signal in Fig. 9(c).

TABLE 1

Comparison of Theoretical and Experimental Results

	Sawtooth wave force			Square wave force		Two 30 Hz cosinoidal stresses		30 Hz and 50 Hz cosinoidal stresses	
Theoretical value (Hz)	30.29	59.66	89.95	30.29	89.95	29.3	29.3	29.3	49.8
Measured value (Hz)	29.37	57.82	89.02	29.37	89.94	30.05	29.11	30.05	49.77
Absolute error (Hz)	0.92	1.84	0.93	0.92	0.01	0.75	0.19	0.75	0.03

fringe and four interference fringes induced by two dynamic stresses. Since the interference fringes of dynamic coupling points are symmetrical about the central fringe, we only take two interference fringes on one side of the central fringe for frequency demodulation.

We applied two dynamic stresses with same frequencies or different frequencies to the PMF and measured simultaneously. The experimental results are shown in Figs. 10 and 11. In Fig. 10, the frequencies of two dynamic stresses are both 30 Hz, and the amplitudes of driving voltages for A and B are 1 V and 250 mV, respectively. In Fig. 11, the frequencies of driving voltages for A and B are 30 Hz and 50 Hz, and the amplitudes of voltages for A and B are 1 V and 250 mV.

It can be seen from Figs. 10 and 11, dynamic stresses with same frequencies or different frequencies can be measured by the DPC system simultaneously. In the time frequency distribution
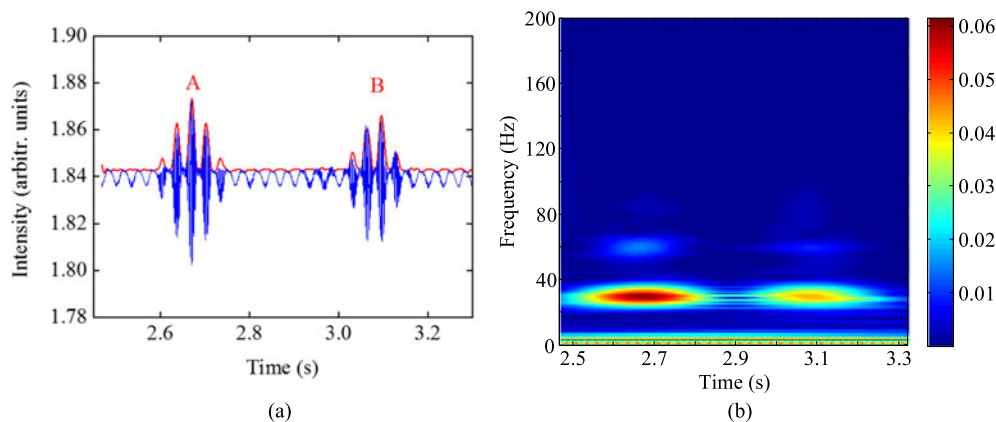
Fig. 10. Experimental results of two 30 Hz cosinoidal forces measurement. (a) Measured interferogram; (b) The time-frequency distribution image of envelop in Fig. 10(a).
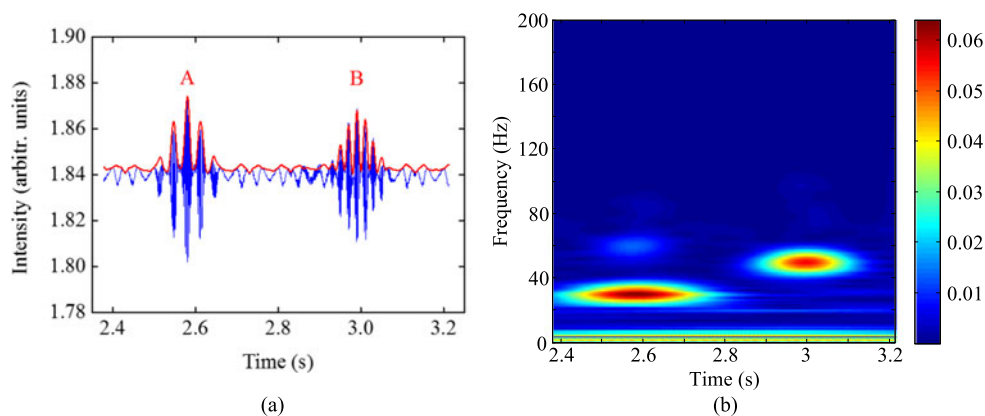

Fig. 11. Experimental results of two cosinoidal forces with frequency of 30 Hz and 50 Hz. (a) Measured interferogram; (b) The time-frequency distribution image of envelop in (a).

images, dynamic coupling points at different fiber sections can be identified because they will separate with each other. The frequency components in Figs. 10(b) and 11(b) are also listed in Table 1, and the frequency measurement errors for two dynamic stresses are less than 0.75 Hz.

4. Discussion

In our experiments, the absolute error of frequency measurement is less than 1.84 Hz. Factors that may account for the frequency errors may arise from four aspects. Firstly, the wavelet transform calculate a discrete time-frequency distribution, there are deviation between calculated frequency value and the real frequency value. We can increase the scale parameter of wavelet transform to make the calculation more accurate. However, the larger scale parameter will lead to larger computation amount and longer computing time. Secondly, the main source of error for low frequency stress measurement is the overlap of measured frequency component and the inherent frequency component. In Figs. 7, 9(b), (d), 10(b) or 11(b), there is an inherent frequency component (2.753 Hz) which is very close to the DC component. The inherent frequency will overlap with the measured frequency when the frequency of stress is small and result in measurement error. Thirdly, the hysteresis of PZT makes noises to interference signal especially for sawtooth wave and square wave. Comparing the time-frequency distribution images of single dynamic coupling point, we find that there are greater noises in Fig. 9(b) and (d) than Fig. 7. This is because the voltage saltations in sawtooth wave and square wave make PZT oscillate fast, and the displacement of PZT exhibits
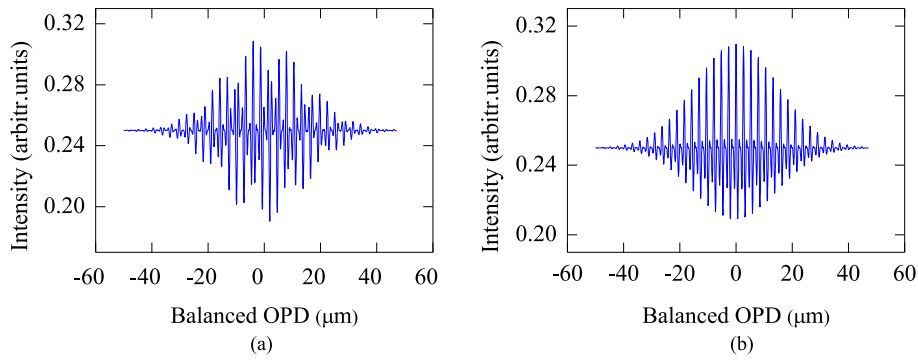
Fig. 12. Deformed interferograms for cosinoidal stresses in case of high frequencies. (a) $\upsilon = 170\,\text{Hz}$, (b) $\upsilon = 190\,\text{Hz}$.

hysteresis when the voltage applied to the PZT changes fast. As the frequency of PZT increases, the hysteresis of PZT will lead to greater noises in interferograms and time-frequency distribution images. Fourthly, the system noise, such as mechanical scanning vibration, environmental light and circuit noise also have impact on frequency calculation.

In addition, We need to consider the upper and lower limits for frequency measurement of periodic signal in our system. In case of static external stress, the width of envelop in the interferogram depend on the coherent length of the light source. The optical coherence function $\gamma(\Delta x)$ approaches zero quickly when $|\Delta x|$ is greater than coherent length L_c. That is, the absolute value of OPD should be less than L_c, i.e., $|\Delta Z - \Delta n_b L| \leq L_c$. Supposing that the moveable mirror of Michelson interferometer starts moving at the balanced position, ΔZ can be expressed as:

$$\Delta Z = 2 \times t \times v \tag{5}$$

Where t is the scanning times, v is the velocity of moveable mirror. We regard the scanning time of coupling point as the maximum period of dynamic stress because only in this circumstance we can observe the phenomenon of modulation. The scanning time of coupling point can be calculated by:

$$\frac{-L_c + \Delta n_b L}{2v} < t < \frac{L_c + \Delta n_b L}{2v} \tag{6}$$

Therefore, the maximum period we can measure is:

$$\frac{L_c + \Delta n_b L}{2v} - \frac{-L_c + \Delta n_b L}{2v} = \frac{L_c}{v} \tag{7}$$

In our experiment, the lower limits of frequency is 5.9 Hz. When the frequency of external stress is lower than 5.9 Hz, from the interferogram we cannot see the periodically modulated envelop of coupling point, and the frequency of external stress cannot be demodulated from the interferogram.

In the process of simulation, we found that there are harmonics in time-frequency distribution images when frequency of stress is greater than frequency of interference fringe, which will lead to misjudgment of modulation frequency. Therefore, the frequency of interference fringe is treated as the maximum frequency we can measure. The frequency of interference fringe deduced according to (3) and (5) is $2v/\lambda$, which is 381.7 Hz in our system. However, from the experimental and simulation results, the interference fringe of coupling point will be out of shape when the frequency of external stress is greater than a quarter of fringe frequency (as shown in Fig. 12), but the modulation frequency of envelop can still be obtained from deformed interferogram.

In theory, our system can achieve frequency measurement ranging from 5.9 Hz to 381.7 Hz. The frequency range is limited by three factors, the coherent length of light source, the wavelength of light source and the velocity of moveable mirror. By taking measures, the frequency range of system can be enlarged and the upper limit could hopefully reach kHz level. For instance, we can increase the coherent length of light source to decrease the lower limit, or decrease the wavelength of light source to make the upper limit larger for frequency measurement. Moreover, changing the

velocity of moveable mirror have impact both on upper and lower limits. In practical application such as intruder detecting, i.e., a walking person, the frequency are usually as low as a few Hz, in this circumstance we can make the moveable mirror scanning at a low speed. While in crack and vibration detections such as bridges, cranes, engines and dragline booms, tens of Hz to kHz frequency detection is required, and we can make the moveable mirror scanning fast to increase the upper limits of frequency measurement.

Our study focus on the measurement of frequency invariant stresses so far. But the wavelet transform is a powerful technique to track the frequency changes and reflect the relationship between the frequency and time effectively. Theoretically, we can analyze the frequency component of dynamic stress by time-frequency distribution image of wavelet transform even if there are multiple frequency components exists in the meantime or the frequency of dynamic stress is time-varying.

5. Conclusion

We proposed a dynamic polarization coupling measurement system based on white light interferometry in this paper. The simulation results shows that the interference fringes of dynamic coupling point are modulated periodically, and the modulation frequency shows linear relationship with frequency of external stress. Wavelet transform is used to get the time-frequency distribution image of envelops extracted from interferogram. Our experiment successfully measured the cosinoidal dynamic coupling point from 10 Hz to 180 Hz with absolute error less than 1.38 Hz and dynamic coupling points of sawtooth wave and square wave with absolute error less than 1.84 Hz. In addition, the DPC system achieved the measurement of two cosinoidal dynamic coupling points simultaneously. In the end, we analyzed the upper and lower limits for frequency measurement in our system, the affecting factors are wavelength of light source, coherent length of light source and the velocity of moveable mirror. Corresponding measures can be taken to enlarge the range of frequency, and this is the next step of our work.

References

[1] Z. W. Guo, H. X. Zhang, and X. W. Chen, "Influence of vibration disturbance during polarization coupling measurement of polarization-maintaining fiber," *Appl. Opt.*, vol. 50, no. 20, pp. 3553–3558, 2011.

[2] X. W. Chen, W. T. Ye, and H. X. Zhang, "Spectral domain demodulation of fibre optics position and displacement sensors by Fourier-transform spectral interferogram," in *Proc. 9th Int. Conf. Opt. Commun. Netw., Nanjing, China*, 2010, pp. 24–27.

[3] D. Y. Song, Z. Y. Wang, and X. W. Chen, "Influence of ghost coupling points on distributed polarization crosstalk measurements in high birefringence fiber and its solution," *Appl. Opt.*, vol. 54, no. 8, pp. 1915–1925, 2015.

[4] H. X. Zhang, W. T. Ye, and X. W. Chen, "Coupling intensity measurement based on white light interferometry in the distributed long PMF sensors," *IEEE Sensors J.*, vol. 12, no. 9, pp. 2905–2909, Sep. 2012.

[5] F. Tang, X. Z. Wang, and Y. M. Zhang, "Characterization of birefringence dispersion in polarization-maintaining fibers by use of white-light interferometry," *Appl. Opt.*, vol. 46, no. 19, pp. 4073–4080, 2007.

[6] Z. H. Li, X. S. Yao, and X. J. Chen, "Complete characterization of polarization-maintaining fibers using distributed polarization analysis," *J. Lightw. Technol.*, vol. 33, no. 2, pp. 372–380, 2015.

[7] S. Chung, J. Kim, and B. A. Yu, "A fiber Bragg grating sensor demodulation technique using a polarization maintaining fiber loop mirror," *IEEE Photon. Technol. Lett.*, vol. 13, no. 12, pp. 1343–1345, Dec. 2001.

[8] T. A. Berkoff, M. A. Davis, and A. D. Kersey, "Fiber optic sensors for distributed vibration monitoring," *SPIE Vibration Monitoring Control*, vol. 2264, pp. 148–154, 1994.

[9] K. Hotate and S. S. L. Ong, "Distributed fiber Brillouin strain sensing by correlation-based continuous-wave technique: Cm-order spatial resolution and dynamic strain measurement," *Proc. SPIE*, vol. 4920, pp. 299–310, 2002.

[10] S. Wang, X. Y. Fan, and Q. W Liu, "Distributed fiber-optic vibration sensing based on phase extraction from time-gated digital OFDR," *Opt. Exp.*, vol. 23, no. 26, pp. 33301–33309, 2015.

[11] J. Zhang and V. A. Handerek, "Distributed sensing of polarization mode coupling in high birefringence optical fibers using intense arbitrarily polarized coherent light," *J. Lightw. Technol.*, vol. 15, no. 5, pp. 794–802, 1997.

[12] M. V Subbarao and P. Samundiswary, "Time-frequency analysis of non-stationary signals using frequency slice wavelet transform," in *Proc. 10th Int. Conf. Intell. Syst. Control*, 2016, pp. 1–6.

[13] Z. S. Li, "Design and analysis of improved Butterworth low pass filter," in *Proc. 8th Int. Conf. Electron. Meas. Instruments*, 2007, pp. 729–732.